Reprinted from *Estuarine, Coastal and Shelf Science* (1982) **14**, 251–263

Ebb-tidal Flow Characteristics near Inlets

Emin Özsoy[a] **and Ümit Ünlüata**[a]

Coastal and Oceanographic Engineering Laboratory, University of Florida, Gainesville, Florida 32611, U.S.A.

Received 10 May 1978 and in revised form 15 March 1981

Keywords: tidal inlets; turbulence; jets; tidal friction; mixing; entrainment

The characteristics of turbulent jets issuing from tidal inlets are analysed by taking into account lateral mixing and entrainment, bottom friction, one-dimensional bathymetric changes and ambient currents. In the absence of depth variations, the jet expansion is exponential as a result of bottom friction. Increasing depths significantly counteract the rapid expansion due to friction, and there are circumstances in which the jet can go through stages of expansion and contraction with distance. Cross-currents in the receiving water body reduce the jet expansion rate and deflect it sideways. These and other results are discussed under the light of qualitative observations.

Introduction

The prediction and understanding of tide-induced currents in coastal waters extending from the continental shelf to the limits of tide-waters in bays and estuaries is a practical task of importance. These currents are especially significant in the vicinity of tidal inlets and estuary mouths for they affect navigation, interior water quality and morphologic changes.

The residual currents generated over much larger times than the tidal period dominate the transport mechanisms especially in micro- and meso-tidal estuaries. This mode of transport determines the rate of sand trapping from the adjacent littoral system (Dean & Walton, 1975) and the equilibrium morphology of the estuary mouth (Hayes & Kana, 1976). The non-linear generation of residual currents described by Dean & Walton (1975), indicate that the lateral entrainment into an expanding jet during ebb and the radial inflow during flood result in the transport of littoral sediments which are partly jetted offshore and partly carried into the interior waters to form extensive shoals. Near some Florida inlets, the net extraction of sand from the littoral system has caused 600-m retrogressions of the shoreline within a period of 50 years (Dean & Walton, 1975). Residual circulations are also very important in determining the flushing characteristics of interior waters, since inlet mouths serve as interfaces between these waters and the exterior (Taylor & Dean, 1974).

Tidal inlet environments show great variability in their characteristics. For example, when freshwater runoff is present, even slight density contrasts can alter the transport mechanisms considerably (Sonu & Wright, 1975). Furthermore, interactions with the bottom are usually very strong. Because of these complexities, there has been a lack of exhaustive analyses in the

[a]Present address: Department of Marine Sciences, Middle East Technical University, P.K.28, Erdemli, Icel, Turkey.

0272–7714/82/030251+16 $03.00/0

past. The attempt by French (1960) is inadequate in that the effects of bottom topography and friction are neglected. The analysis of the exchange characteristics by Taylor & Dean (1974) has also been limited by the assumption of zero jet entrainment and constant depth, although they have included bottom friction.

In the present work we restrict our attention to ebbing flows from micro-tidal inlets with negligible freshwater inflow. The cases to be studied may indeed be representative of a small subset of inlets, and therefore our purpose will be to study certain processes of primary importance, keeping in mind the possible modifications to the model in the presence of other effects such as stratification, wave-induced drift currents etc. The bottom topography is represented by arbitrary one-dimensional variations in the offshore direction. The lateral variations of bathymetry are not included, but, because of the integral method used in the analysis, these variations are accounted for in an average sense (although a more general solution may be obtained by numerical methods) assuming the transverse variations to be small with respect to the depth scale (micro-tidal estuaries). The effects of bottom friction and weak cross-currents are included. The depth-averaged equations of motion are solved analytically, using the assumptions of quasi-steadiness and self-similarity. The effects of and interactions between frictional resistance, variable bottom topography and cross-currents are studied in detail. The effects of earth's rotation, density stratification and unsteady development are discussed only in a general qualitative sense.

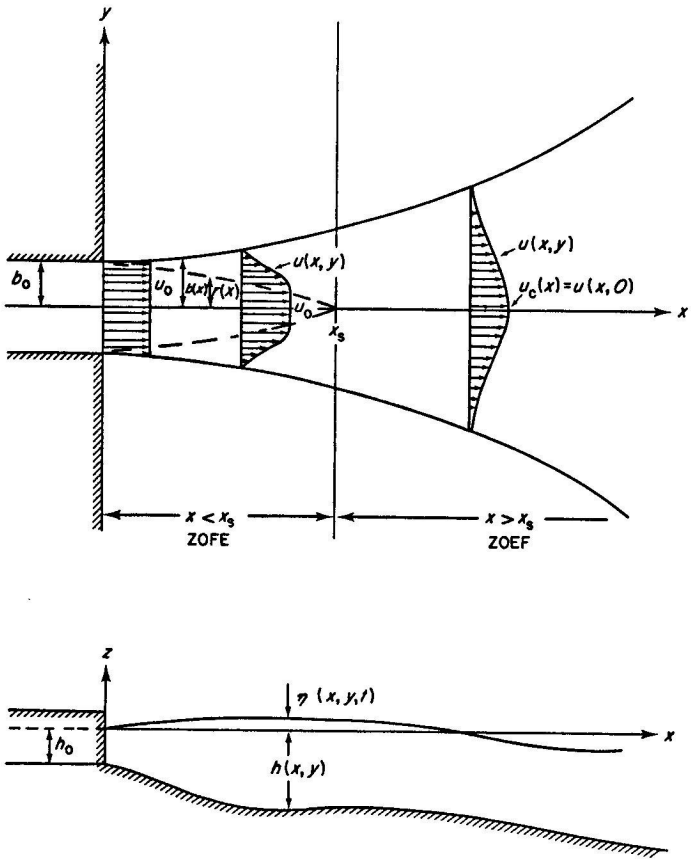

Figure 1. Definition sketch.

Shallow water jet analysis

We consider the turbulent jet flow produced by the water ebbing from an inlet into a semi-infinite ocean in Figure 1. The approximate equations of motion (see Appendix A) for the jet region are

$$\frac{\partial hu^2}{\partial x} + \frac{\partial huv}{\partial y} = -\frac{f}{8}u^2 + \frac{1}{\rho}\frac{\partial}{\partial y}Fyx, \tag{1a}$$

$$\frac{\partial hu}{\partial x} + \frac{\partial hv}{\partial y} = 0. \tag{1b}$$

The classical two-dimensional turbulent jet equations (Schlichting, 1968) can be recovered directly by setting $f = 0$, $h = h_0 =$ constant in equations (1a, b).

In order to solve equations (1a, b) for the jet half-width $b(x)$, the core width $r(x)$ and the centerline velocity $u_c(x)$, the velocity distribution $u(x,y)$ in Figure 1 is assumed to be self-similar with respect to the normalized coordinate $\zeta = |y|/b(x)$. The particular similarity profile $u/u_c = F(\zeta)$ is adopted from Abramovich (1963) and Stolzenbach & Harleman (1971) as

$$F(\zeta) = \begin{cases} 0 & ; 1 < \bar{\zeta} \\ (1-\bar{\zeta}^{1.5})^2 & ; 0 < \bar{\zeta} < 1, \\ 1 & ; \bar{\zeta} < 0 \end{cases} \quad \bar{\zeta} = \frac{\zeta - r/b}{1 - r/b}. \tag{2}$$

To distinguish between the Zone of Flow Establishment (ZOFE) and the Zone of Established Flow (ZOEF) in Figure 1, it is sufficient to set $r = 0$ ($\bar{\zeta} = \zeta$) in equation (2) in the ZOFE ($x > x_s$, see Figure 1), since the core region ends at $x = x_s$. In the absence of experimental data, it is difficult to assess the validity of either the self-similarity assumption or the choice of a particular distribution for the present application; however, the above assumptions have led to reasonable results elsewhere (Stolzenbach & Harleman, 1971), and quite often the choice of a profile is immaterial for the gross jet properties in the near field.

The two-dimensional mouth morphology is often very complicated and may interact strongly with the currents, especially at meso-tidal inlets (Hayes & Kana, 1976). Since we will be using integral jet equations to study mainly micro-tidal inlets, depth averages in the transverse direction will be used. Allowing only one-dimensional variations in depth: $h = h(x)$, we integrate equations (1a, b) across the jet. The velocity u and the shear force F_{xy} vanish as $y \to b$, but there exists a lateral entrainment velocity $v_e = au_c$, where a is the entrainment coefficient, defined by Morton *et al.* (1956). Introducing the normalized variables

$$\xi = \frac{x}{b_0}, \ \mu = \frac{fb_0}{8h_0}, \ H(\xi) = \frac{h}{h_0}, \ R(\xi) = \frac{r}{b_0}, \ B(\xi) = \frac{b}{b_0}, \ U(\xi) = \frac{u_c}{u_0}, \tag{3a–f}$$

where b_0, h_0 and u_0 are respectively the half-width, depth and velocity at the inlet, two ordinary differential equations are obtained:

$$\frac{d}{d\xi}(\bar{I}_2 HBU^2) = -\mu \bar{I}_2 BU^2 \text{ and } \frac{d}{d\xi}(\bar{I}_1 HBU) = aHU. \tag{4a, b}$$

By virtue of equation (2), $\bar{I}_n$ are defined as

$$\bar{I}_n(\xi) = \int_0^1 F^n(\zeta)d\zeta = \frac{R}{B} + I_n\left(1 - \frac{R}{B}\right); \ n = 1,2, \tag{5}$$

where $I_1 = 0{\cdot}450$ and $I_2 = 0{\cdot}316$ are the constant values of I_1 and I_2 in the ZOEF, since $R = 0$ in this zone.

The solutions to equations (1a) and (1b) are obtained in Appendix B. The classical jet solutions in which the jet width grows linearly and the velocity decays as $\xi^{-\frac{1}{2}}$ (Albertson *et al.*, 1950; Abramovich, 1963; Schlichting, 1968) are recovered easily by setting $\mu = 0$ and $H = 1$ in equations (B.5a, b). Values of the entrainment coefficient a are obtained by comparing these solutions with the observed values of the growth rates.

$$\varepsilon_1 = \frac{\mathrm{d}(B-R)}{\mathrm{d}\xi} = \frac{a}{I_1 - I_2} \quad \text{and} \quad \varepsilon_2 = \frac{\mathrm{d}B}{\mathrm{d}\xi} = \frac{2a}{I_1} \tag{6}$$

within the ZOFE and ZOEF, respectively. Stolzenbach & Harleman (1971) have determined a by taking $\varepsilon_1 = \varepsilon_2 = 0{\cdot}22$ in equation (6). We have used Abramovich's (1963) observations of $\varepsilon_1 = 0{\cdot}27$ and $\varepsilon_2 = 0{\cdot}22$ respectively to obtain $a = a_1 = 0{\cdot}036$ for $\xi < \xi_s$ and $a = a_2 = 0{\cdot}050$ for the region $\xi > \xi_s$. These values lead to a satisfactory agreement with the classical jet solutions as observed in Figure 2.

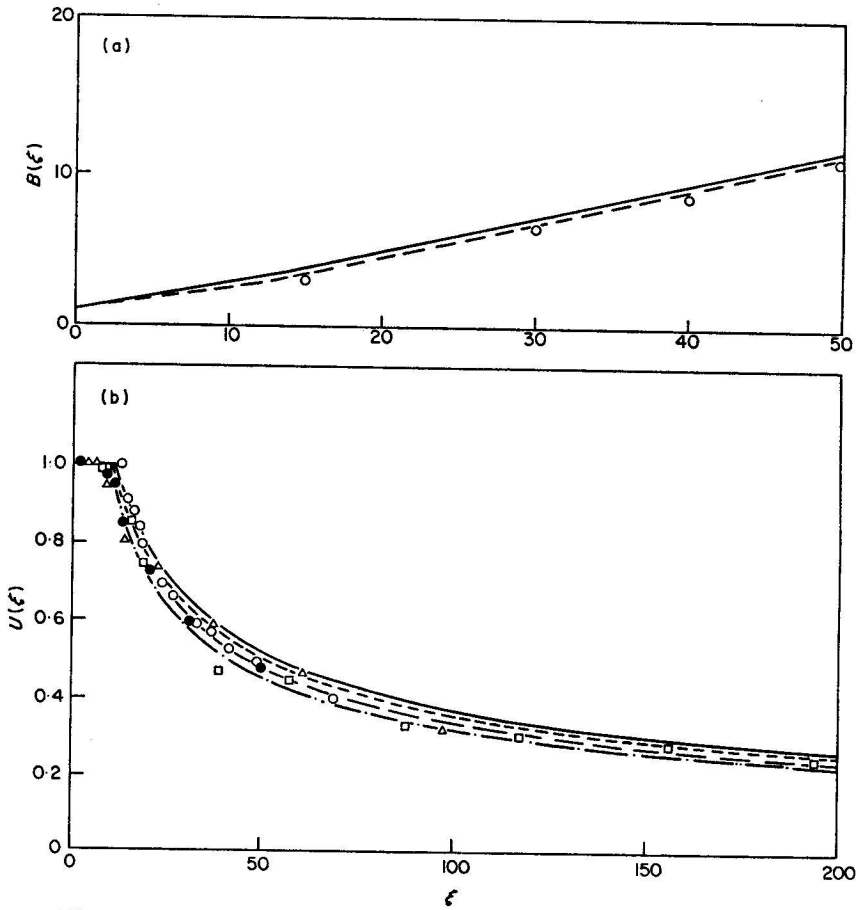

Figure 2. Comparison with classical jets for $\mu = 0$, $H = 1$. (a) Jet half-width, (b) centerline velocity. Experimental data: Förthmann (after Abramovich, 1973), ○; Albertson *et al.* (1950), △ ($u_0 = 40$ ft s^{-1}, $b_0 = \frac{1}{8}$ in), ● ($u_0 = 100$ ft s^{-1}, $b_0 = \frac{1}{8}$ in), □ ($u_0 = 160$ ft s^{-1}, $b_0 = \frac{1}{32}$ in). Theoretical solutions: —, present solution; – – – –, Abramovich (1973); — . —, Albertson *et al.* (1950); — — —, Reichardt & Goertler (after Schlichting, 1968).

The effect of bottom friction

The solution for a flat bottom with friction is given by equations (B.6 a,b), The jet width grows and the centerline velocity decays exponentially as $\xi \to \infty$, as opposed to frictionless (classical) jets. The features of the bottom-frictional jet are displayed in Figure 3. The parameter μ combines the effects of the friction coefficient f and the aspect ratio b_0/h_0 such that either effect can cause the rapid jet expansion due to loss of momentum against the bottom resistance. By taking limits of equations (B.3a) and (B.3b) as $\xi \to 0$, it can be shown that the growth rate ε_1 for the shear layer thickness $(B-R)$ in equation (6) becomes $\varepsilon_1 \simeq (a+\mu)/(I_1-I_2)$. This result indicates significant alterations even in the initial portion of the ZOFE since $\mu = O(a)$ typically.

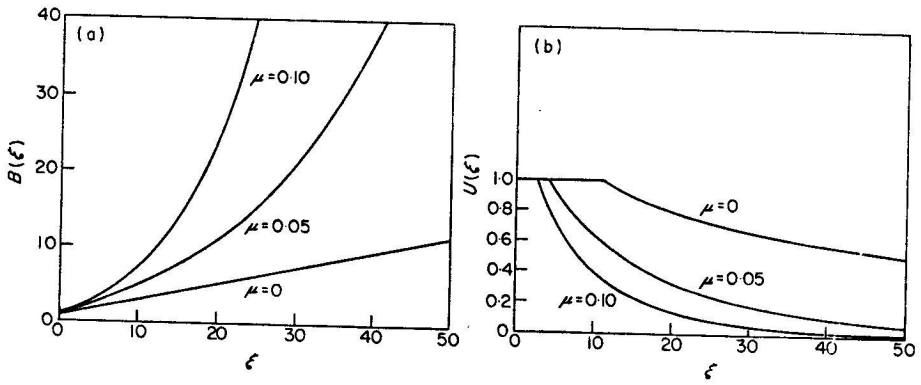

Figure 3. Bottom-frictional jet over a bottom of constant depth. (a) Jet half-width, (b) centerline velocity.

Possible field evidence for the exponential growth of the bottom-frictional jet can be found in Dean & Walton (1975), where the observed ebb currents near Redfish Pass, Florida indicate a rapidly widening jet.

In experimental and analytical studies on jets in rotating systems, Savage & Sobey (1975) and Gadgil (1971) have demonstrated the fast spreading rates of bottom-frictional jets. By neglecting lateral entrainment and mixing, Borichansky & Mikhailov (1966) and Taylor & Dean (1974) have also obtained the exponential dependence of the jet width and velocity on distance. The former authors are led to erroneous results by assuming the jet momentum to be conserved as opposed to the present work. Due to their simplifying assumptions, the latter authors find that the jet width grows as $e^{\mu\xi/2}$, whereas the growth in the present solution is shown to be as $e^{\mu\xi}$. This faster growth rate is due to the additional effect of entrainment and lateral mixing, as remarked earlier.

Jets on a sloping bottom

We now consider linear variations in depth by taking $H = 1+\nu\xi$, where $\nu = mb_0/h_0$, m being the bottom slope. In the solutions (B.7a, b) the effects of depth variations, bottom friction and the lateral entrainment on the dynamics of the jet are expressed, respectively, by ν, μ and a. We have already considered the roles of the parameters μ and a by setting $\nu = 0$. If we now take $\mu = 0$, $a = 0$ in equation (B.7), we obtain $B = 1/I_2H$ and $U = 1$, that is, with increasing depth, the jet contracts due to mass conservation and the centerline velocity remains constant, as predicted by Arthur (1962).

We next take $a \neq 0$ but keep $\mu = 0$; that is, allow for lateral entrainment, in which case the solution indicates a contraction in jet width near $\xi = \xi_s$ and a linear growth as $\xi \to \infty$. However, this result holds for $\nu > 0$, and for the opposite case, $\nu < 0$ (decreasing depth), the bottom intersects the water surface at $\xi = 1/|\nu|$, near which the jet grows as $B \sim 1/H$ due to contributions of both depth decrease and lateral entrainment.

On the other hand, taking $a = 0$ and $\mu \neq 0$ it is seen that the jet width depends critically on the ratio μ/ν. For positive slopes ($\nu > 0$), the jet will contract if $\nu > \mu$ and expand if $\nu < \mu$. In the former situation contraction due to the depth effect is suppressing the jet expansion resulting from the bottom friction, while in the latter case bottom friction is dominant. When $\mu = \nu$, a balanced condition is reached, in which the jet width remains constant with offshore distance. Finally for $\nu < 0$, the jet expansion is enhanced by the decrease in depth.

It is clear from the preceding discussions of the various limiting cases that, under the more general circumstances ($a \neq 0$, $\mu \neq 0$), the effect of increasing depth is to counteract the effects of bottom friction and lateral entrainment. For decreasing depth with distance offshore, the three effects will be acting the same way to lead to the expansion of the jet. These points are further illustrated in Figure 4 keeping ν as parameter and fixing the values of μ and a.

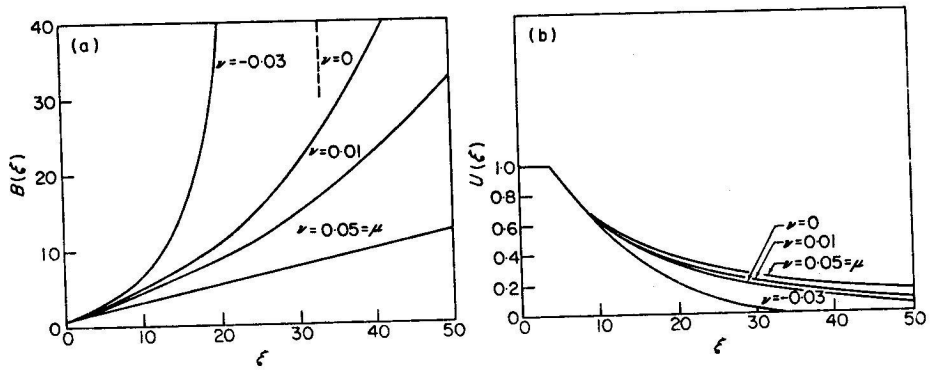

Figure 4. Jet characteristics over a linearly varying bottom topography, $\mu = 0{\cdot}05$. (a) Jet half-width, (b) centerline velocity. The dashed line is the asymptote for $\nu = -0{\cdot}03$.

It is seen that the effect of bathymetric variations on jet expansion are overwhelming, because, even for slopes as small as that corresponding to $\nu = 0{\cdot}01$, the exponentially growing extent of the bottom-frictional jet is altered significantly. The velocity, however, does not exhibit any significant variations with ν. It is worth noting that for $\mu = \nu$, i.e. when the bottom friction and depth effects are in balance, equations (B.7a, b) indicate a linearly expanding jet (due to lateral entrainment alone) as in the case of a classical jet. The velocity variations, however, differ from the classical jet, because the decay here is as $H^{-3/2}$, hence faster.

An apparent singularity is detected in the jet expansion when $2\nu = \mu$ in equation (B.7a). Upon carrying out the limit as $\mu \to 2\nu$ it is seen that the jet grows linearly near the inlet ($H \simeq H_s$), but the growth is logarithmic as ($H \ln H$) at large distances away from the inlet.

In conclusion, it can be stated that depending on the relative orders of magnitude of the parameters μ, ν and a, the behavior of the jet is changed dramatically from an exponential to a linear, then to a logarithmic behavior.

Arbitrary depth variations

In order to investigate further the interplay between the frictional and bathymetric effect, we provide a rough comparison of the present results with what can be obtained from aerial photographs of an actual inlet.

Aerial photographs of Jupiter Inlet, Florida (Plate 1) taken on a relatively calm day in June 1973 are unique in showing the jet boundary clearly. The bathymetric map of the inlet's vicinity is shown in Figure 5. Using Figure 5, it can be inferred from the aerial photographs that the jet expands in passing over the shoals and contracts afterwards as the depth increases.

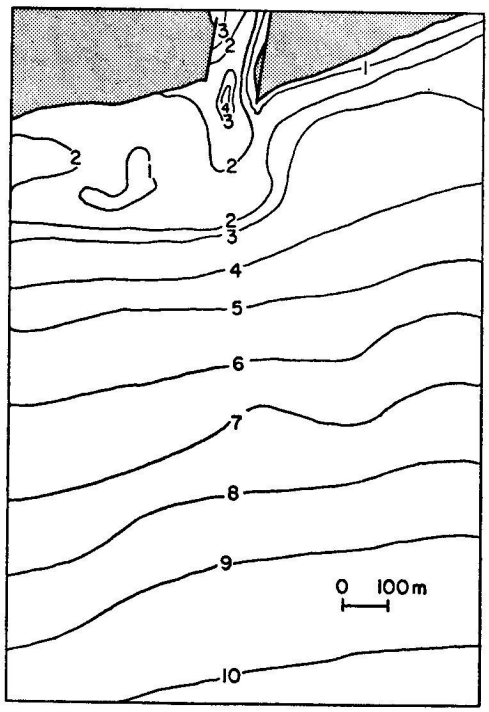

Figure 5. Bathymetric map of Jupiter Inlet, and vicinity (depth in m based on 1967 data, U.S.G.S.).

A sample calculation is made by using an average 1-dimensional depth variation shown on the top of Figure 6, and integrating equations (B.1), (B.2) and (B.4) by numerical quadrature. The inlet half-width and depth are $b_0 = 50$ m and $h_0 = 3$ m, respectively. A friction coefficient of $f = 0{\cdot}02$ was assumed, implying $\mu = 0{\cdot}04$. The calculated variation of the jet width is compared in Figure 6 with its actual values estimated from the aerial photographs after correcting for perspective viewing. In view of the uncertainties, the results seem to be satisfactory.

Jets in cross-currents

Alongshore currents generated by winds, waves or tides often deflect tidal jets, as shown in Plate 2. Although the coastline attached flows [Plate 2(a)] require more detailed studies, the present method of analysis can readily be applied to gradually bending jets [Plate 2(b)], when the alongshore velocity $u_a \ll u_0$.

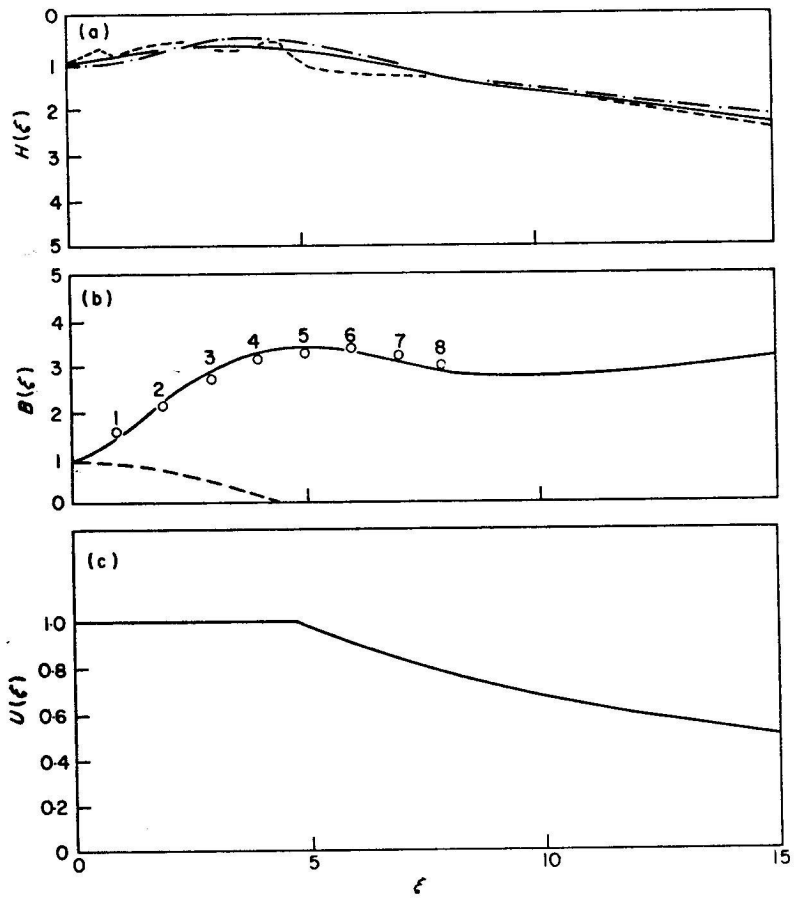

Figure 6. Comparison with the jet characteristics at Jupiter Inlet (a) Depth variations (– – –, 1975 data by the State of Florida, D.N.R.; — . —, 1967 data; ——, present solutions. (b) Jet half-width. Data points 1–8 are obtained from photograph in Figure 5. The dashed line outlines the core region of the jet. (c) Centerline velocity.

The equations for slightly curved jets are developed in Appendix C for the geometry shown in Figure 7. Numerical solutions are shown in Figure 8. The centerline velocity has not been included since no appreciable change has been observed. However, the jet expansion is seen to be reduced due to the co-flowing component of the cross-current, as the jet is deflected sideways. The cross-current U_A is taken as constant in these examples, although offshore variations in the cross-current can be allowed in general.

Discussion and conclusions

The reader must be cautioned against some of the limitations of the present analyses. It is expected that, for steep bottom slopes, adverse pressure gradients will force the entire flow to be separated from the bottom at an offshore location. For steeper bottom slopes, the flow will initially lose contact with the bottom. In this limit, neither the analysis nor the conclusion with regard to jet contraction caused by depth increase will be valid.

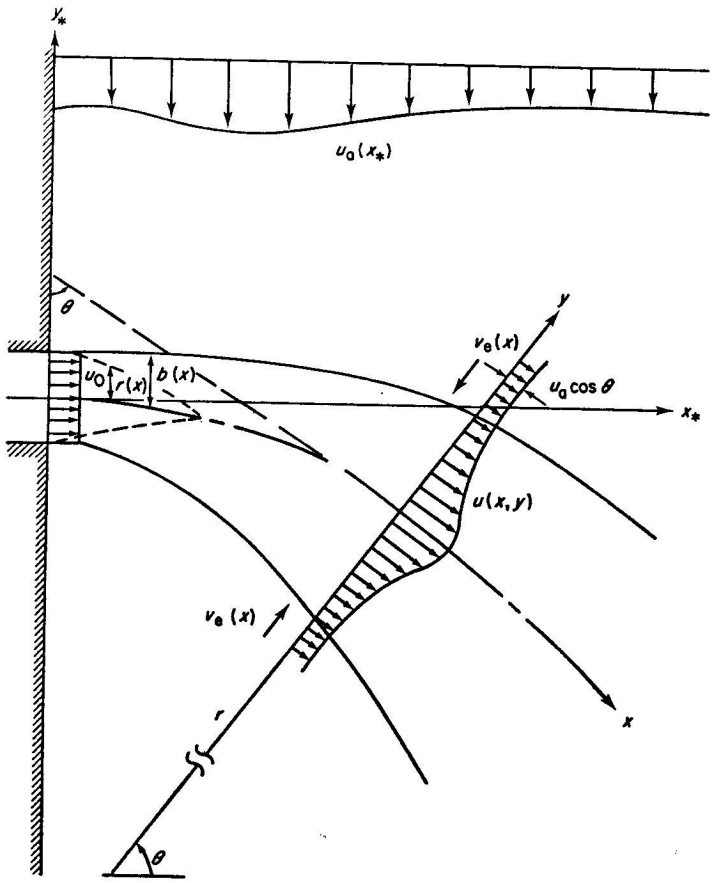

Figure 7. Definition sketch for jets in cross-currents.

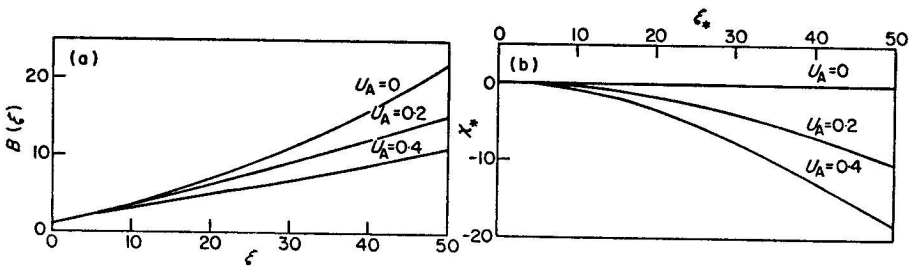

Figure 8. Jets in cross-currents: (a) jet half-width, (b) centerline trajectory.

Buoyant freshwater originating in the adjacent bay or lagoon waters contributes to the separation of the flow from the bottom (Wright & Sonu, 1974; Sonu & Wright, 1975), as in the case of river plumes (Wright & Coleman, 1974; Garvine, 1977). If separation does not occur in the immediate vicinity of the river mouth or tidal inlet, the present solutions will be applicable, since the effects of bathymetric changes and bottom friction are shown to be quite significant in this region by Wright & Coleman (1974), Wright & Sonu (1974) and Wright (1976).

Tidal jets often extend many km offshore. Therefore, rotational effects will be felt when Rossby number $Ro \equiv u_0/\beta l = O(1)$. However, for shallow water jets (jets covering the full depth), the effects of the earth's rotation are negligible in the main part of the fluid, since analytical and experimental investigations by Gadgil (1971) and Savage & Sobey (1975) indicate that the jet path remains straight in spite of the Coriolis forces. The effects of rotation are most strongly felt near Ekman boundary layers (Gadgil, 1971), which may somewhat modify the bottom friction included in the present analysis. In the presence of depth variations, one may anticipate additional effects of the earth's rotation on shallow water jets, due to conservation of potential voiticity (Greenspan, 1969). On the other hand horizontal jets in deep water are found to be deflected due to Coriolis forces (Savage & Sobey, 1975). A simpler analysis of this kind, applicable to buoyant river plumes, has been performed by Takano (1955).

The present quasi-steady jet analysis also does not predict the unsteady jet features shown in Plate 3. Turner (1962), Tsang & Wood (1968), Tsang (1970) and Middleton (1975) have analysed the buoyant starting plume as a composite of a steady, fully developed jet and an unsteady thermal.

In our analysis the effects of turbulent entrainment, bottom friction, topography and cross-currents are emphasized due to their primary importance in determining the current patterns near a micro- or meso-tidal estuary mouth. The ebb-tidal currents are found to depend crucially on the local bathymetry and bottom friction as well as on entrainment. The behaviour of bottom-frictional jets on variable topography differ completely from the classical jet behaviour. Bottom friction retards the flow and depth increase in the offshore direction counteracts the frictional expansion in preserving the coherent flow structure. On the other hand, when the flow may be passing over shoals, bottom friction and shallowness act together to expand the jet. Rough comparisons support the analyses, but there is little doubt that there is an urgent need for field and laboratory data before further statements can be made with confidence.

The results are clearly applicable to narrow estuary mouths experiencing sufficiently large tidal excursions through them (i.e. micro- and meso-tidal environments) and whenever the freshwater inflow and wave incidence are insignificant. In the case of meso-tidal inlets where there is a strong interaction with bottom features, the solutions may only be indicative of gross jet properties such as the jet width, since the actual velocity profiles must be altered significantly. The average value of depth in the transverse direction used in the analysis is sufficiently representative when two-dimensional interactions are expected to be weak.

In actuality the bottom interaction is radically changed by sediment transport. Tidal deltas evolve as a result of transport, and in return they modify the currents in meso-tidal environments (Hayes & Kana, 1976; Dean & Walton, 1975), but this is beyond our scope at present. In a forthcoming paper we will be considering the suspended sediment transport by tidal jets.

Acknowledgements

We are grateful to Dean Morton Smutz for his kind support and encouragement. The photographs are courtesy of Coastal Engineering Archives at U.F.

References

Abramovich, B. N. 1963 *The Theory of Turbulent Jets*. MIT Press, Cambridge, Massachusetts.

Albertson, M. L., Dai, Y. B., Jensen, R. A. & Rouse, H. 1950 Diffusion of submerged jets. *Transactions of the American Society of Civil Engineers* **115**, 639.

Plate 1. Jet development at Jupiter Inlet, Florida (1973 photograph).

[*Facing p. 260*

Plate 2. Effects of cross-currents: (a) strong alongshore wave-induced currents at South Lake Worth Inlet, Florida, (b) weak cross-currents at Bakers Haulover Inlet, Florida.

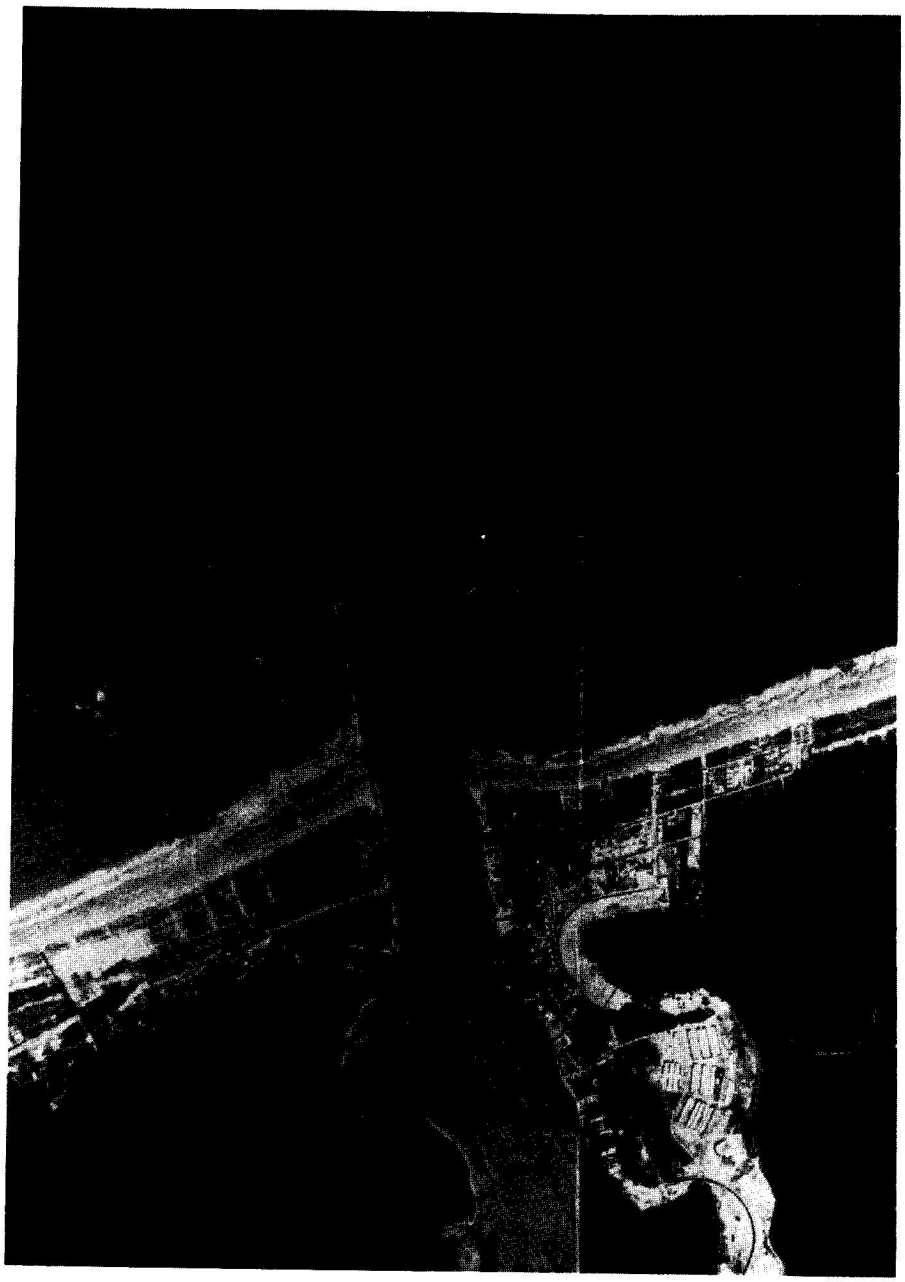

Plate 3. Starting tidal jet at Forth Pierce Inlet, Florida.

Arthur, R. S. 1962 A note on the dynamics of rip currents. *Journal of Geophysical Research* **67**, 2777–2779.
Borichansky, L. S. & Mikhailov, V. N. 1966 Interaction of river and sea water in the absence of tides. *Scientific Problems of the Humid Tropical Zone Deltas and their Implications.* UNESCO, Paris. pp. 175–180.
Dean, R. G. & Walton, T. L. 1975 Sediment transport processes in the vicinity of inlets with special reference to sand trapping. In *Estuarine Research*, Volume 2 (Cronin, L. E., ed.). Academic Press, New York.
Dronkers, J. J. 1964 *Tidal Computations.* North Holland, Amsterdam.
French, J. L. 1960 Tidal flow in entrances. *U.S. Army Corps of Engineers, Committee on Tidal Hydraulics, Technical Bulletin No.* 3.
Gadgil, S. 1971 Structure of jets in rotating systems. *Journal of Fluid Mechanics* **47**, 417–436.
Garvine, R. W. 1977 Observation of the motion field of the Connecticut River plume. *Journal of Geophysical Research* **82**, 441–454.
Greenspan, H. P. 1969 *The Theory of Rotating Fluids.* Cambridge University Press, London. 328 pp.
Hayes, M. O. & Kana, T. W. 1976 Terrigenous clastic depositional environments. *University of South Carolina, Technical Report No.* 11-CRD.
Middleton, J. G. 1975 The asymptotic behavior of a starting plume. *Journal of Fluid Mechanics* **72**, 753–771.
Morton, B. R., Taylor, G. & Turner, J. S. 1956 Turbulent gravitational convection from maintained and instaneous sources. *Proceedings of the Royal Society of London Series A* **234**, 1–23.
Özsoy, E. 1977 Flow and mass transport in the vicinity of tidal inlets. *Coastal and Oceanographic Engineering Laboratory, University of Florida, Report No.* TR-036, 196 pp.
Savage, S. B. & Sobey, R. J. 1975 Horizontal momentum jets in rotating basins. *Journal of Fluid Mechanics* **71**, 755–768.
Schlichting, H. 1968 *Boundary Layer Theory*, 6th edition. McGraw-Hill, New York.
Sonu, C. J. & Wright, L. D. 1975 Mass transport and dispersion off a tidal inlet. *Offshore Technology Conference, Paper No.* OTC 2383.
Stolzenbach, K. D. & Harleman, D. R. G. 1971 An analytical and experimental investigation of surface discharges of heated water. *Ralph M. Parsons Laboratory for Water Resources and Hydrodynamics, MIT, Report No.* 135.
Takano, K. 1955 A complementary note on the diffusion of the seaward flow off the mouth of a river. *Journal of the Oceanographical Society of Japan* **11**, 1–3.
Taylor, R. B. & Dean, R. G. 1974 Exchange characteristics of tidal inlets. *Proceedings of the 14th Coastal Engineering Conference.* pp. 2268–2289.
Tsang, G. & Wood, I. R. 1968 Motion of two-dimensional starting plume. *Journal of Engineering Mechanics Division of the American Society of Civil Engineers* **94**, 1547–1561.
Turner, J. S. 1962 The 'starting plume' in neutral surroundings. *Journal of Fluid Mechanics* **13**, 356–368.
Wang, J. D. & Connor, J. J. 1975 Mathematical modeling of near coastal circulation. *Ralph M. Parsons Laboratory for Water Resources and Hydrodynamics, MIT, Report No.* 200.
Wright, L. D. 1976 Morphodynamics of a wave-dominated river mouth. *Proceedings of the 15th Coastal Engineering Conference.* pp. 1721–1737.
Wright, L. D. & Coleman, J. M. 1974 Mississippi River mouth processes: effluent dynamics and morphologic development. *Journal of Geology* **82**, 751–778.
Wright, L. D. & Sonu, C. J. 1974 Processes of sediment transport and tidal development in a stratified tidal inlet. *Estuaries* **2**, 63–76.

Appendix A

The depth-averaged shallow water equations of motion (Wang & Connor, 1975) are:

$$\frac{\partial \eta}{\partial t} + \frac{\partial hu}{\partial x} + \frac{\partial hv}{\partial y} = 0, \tag{A.1a}$$

$$\frac{\partial hu}{\partial t} + \frac{\partial hu^2}{\partial x} + \frac{\partial huv}{\partial y} - \beta hv = -gh\,\frac{\partial \eta}{\partial x} + \frac{1}{\rho}\left[\tau_x^b + \frac{\partial Fxx}{\partial x} + \frac{\partial Fyx}{\partial y}\right], \tag{A.1b}$$

$$\frac{\partial hv}{\partial t} + \frac{\partial huv}{\partial x} + \frac{\partial hv^2}{\partial y} + \beta hu = -gh\,\frac{\partial \eta}{\partial y} + \frac{1}{\rho}\left[\tau_y^b + \frac{\partial Fxy}{\partial x} + \frac{\partial Fyy}{\partial y}\right], \tag{A.1c}$$

where t is the time, (x,y) the horizontal coordinates, η the free surface displacement, h the still water depth, ρ the density, g the gravitational acceleration, β the Coriolis parameter, (u,v) the depth-averaged horizontal velocity, (τ_x^b, τ_y^b) the bottom shear force, and Fxx, $Fxy = Fyx$, Fyy are the components of the depth-integrated stress tensor (including turbulent fluctuations).

The time, length, depth, surface displacement and velocity scales characterizing the jet flow are selected respectively as T_0, L_0, h_0, a_0 and u_0. The scale δL_0 is a measure of the jet width (or boundary layer thickness), so that $v/u = O(\delta) = O(a)$, a being the entrainment coefficient. The bottom shear stresses are expressed (Dronkers, 1964) as $\tau_x^b = (\rho f/8)\, u\sqrt{u^2+v^2} = (\rho f/8)\, u|u| + O(\delta^2/2)$ and $\tau_y^b = (\rho f/8)\, v\sqrt{u^2+v^2} = (\rho f/8)O(\delta)$, where f is the friction factor.

The normal and lateral turbulent stresses are scaled with the factor $\rho u_0^2 \mu^2$ where μ is a measure of the turbulent fluctuations. By scaling the equations with these parameters, it is seen that all of the terms in equation (A.1c) are $O(\delta)$ or smaller, with the result that in the $\partial n/\partial y$ term $a_0 = u_0^2 g^{-1} O(\delta^2)$. Therefore the horizontal pressure gradient terms $\nabla\eta$ are shown to be negligible, as they are 'impressed' on the flow in boundary layer theory. The $\dfrac{\partial \eta}{\partial t}$ and $\dfrac{\partial hu}{\partial t}$ terms in equations (A.1a, b) are $O(a_0 L_0/h_0 u_0 T)$ and $O(L_0/u_0 T)$ respectively. But due to the rapid jet expansion and within the initial region of the jet (<5 km) the ratio of the length scale to the tidal excursion length $L_0/u_0 T_0 \ll 1$. Therefore both of these unsteady terms are neglected. The $O(1)$ terms in bottom stresses and $O(\mu^2/\delta)$ terms in the turbulent stresses are retained. These simplifications lead to equations (1a, b).

Appendix B

Equations (4a, b) are uniformly valid for all ξ. Equation (4a) can be integrated directly to yield

$$\bar{I}_2 HBU^2 = \exp\left\{-\mu \int_0^\xi \frac{d\xi'}{H(\xi')}\right\} \equiv \mathcal{J}(\xi), \tag{B.1}$$

where we have invoked the initial conditions $B(0) = 1$, $R(0) = 1$, $H(0) = 1$, $U(0) = 1$, and have noted that $\bar{I}_2 B \to 1$ as $\xi \to 0$. To integrate equation (5b) in the ZOFE, we set $U = 1$ [see equations (3) and (4)] to obtain

$$\bar{I}_1 HB = a \int_0^\xi H(\xi')\, d\xi' + 1 \equiv G(\xi) \tag{B.2}$$

where it has been noted that $\bar{I}_1 B \to 1$ as $\xi \to 0$. The solutions for the two unknowns R and B in the ZOFE follow from equations (B.1) and (B.2) by setting $U = 1$ in the former equation and utilizing equation (5):

$$R = \frac{I_1 \mathcal{J} - I_2 G}{(I_1 - I_2)H}, \quad B = \frac{(1-I_2)G - (1-I_1)\mathcal{J}}{(I_1 - I_2)H} \tag{B.3a, b}$$

To obtain the solutions for U and B in the ZOEF, we first utilize equation (B.1) and define $\psi = \mathcal{J}/U$ to put equation (4b) into the form $\psi d\psi/d\xi = aI_2 H\mathcal{J}/I_1$, and integrate from $\xi_s = x_s/b_0$ (given by the roots of $R(\xi_s) = 0$) to $\xi > \xi_s$ (noting that $\psi(\xi_s) = \mathcal{J}(\xi_s)$) to yield

$$\psi^2 = \frac{\mathcal{J}^2}{U^2} = \frac{2aI_2}{I_1} \int_{\xi_s}^\xi H(\xi')\mathcal{J}(\xi')d\xi' + \mathcal{J}^2(\xi_s) \equiv L(\xi). \tag{B.4}$$

From equations (B.1) and (B.4) it follows that

$$U = \mathcal{J}L^{-1/2} \text{ and } B = L/I_2H\mathcal{J}. \tag{B.5a, b}$$

For the limiting case of constant depth ($H = 1$), the solution in equation (B.5b) (ZOEF) reduces to

$$B = \frac{e^{\mu\xi}}{I_2}\{e^{-2\mu\xi_s} + \frac{2aI_2}{\mu I_1}(e^{-\mu\xi_s} - e^{-\mu\xi})\},\ U = e^{-\mu\xi}\Phi^{-1/2} \tag{B.6a, b}$$

where Φ stands for the expression in the curly brackets.

On the other hand, if a linear depth variation $H = 1 + \nu\xi$ is assumed, the general solutions reduce to

$$B = \frac{H^{\mu/\nu-1}}{I_2}\{H_s^{-2\mu/\nu}\ \frac{2aI_2}{I_1(2\mu-\nu)}(H^{2-\mu/\nu} - H_s^{2-\mu/\nu})\}\ U = H^{-\mu/\nu}\Phi^{-1/2} \tag{B.7a,b}$$

in the ZOEF, with Φ representing the terms in the curly brackets and $H_s = H(\xi_s)$.

Appendix C

Following Stolzenbach & Harleman (1971), we adopt the locally cylindrical coordinates shown in Figure 7, and retain equation (1.c) and the lateral pressure forces. By making use of the Bernoulli equation relating velocities at the jet boundaries $y = \pm b$ to those at $y \to \pm\infty$, the pressure forces responsible for deflecting the jet can be integrated laterally, yielding

$$-gh\int_{-b}^{+b}\frac{\partial\eta}{\partial y}\,dy = -gh\,[\eta(b) - \eta(-b)] = 2hv_e u_a \sin\theta, \tag{C.1}$$

where $u_a \sin\theta$ is the lateral component of the cross-current at $y \to \pm\infty$. The integration of equation (A.1a–c) lead to equations that are the same as equations (4a, b) in the coordinates of Figure 7 with the addition of the term $aHU_AU\cos\theta$ to the right hand side of Equation (4a), where $U_A = u_a/u_0$. The lateral integration of the momentum equation in the direction perpendicular to the jet axis yields

$$\bar{I}_2HBU^2\frac{d\theta}{d\xi} = -aHU_AU\sin\theta. \tag{C.2}$$

By relating $\xi_* = x_*/b_0$ and $\chi_* = y_*/b_0$ to the curvilinear coordinate $\xi = x/b_0$, two additional equations are obtained:

$$\frac{d\xi_*}{d\xi} = \sin\theta, \text{ and } \frac{d\chi_*}{d\xi} = \cos\theta. \tag{C.3a, b}$$

In the preceding equations, the velocity profiles are assumed to be self-similar and symmetrical, based on the assumption of gradual jet bending. The modifications in the similarity profiles due to the co-flowing component ($u_a\cos\theta$) of the cross-current are then expressed as $F(\xi) = (u - u_a\cos\theta)/(u_c - u_a\cos\theta)$, and therefore, the functions $\bar{I}_1$ and $\bar{I}_2$ in equation (5) have to be modified accordingly.

Printed in Great Britain by Henry Ling Ltd., at the Dorset Press, Dorchester, Dorset